

# Digital-Carrier Multi-Band User Codes for Baseband UWB Multiple Access

Liuqing Yang and Georgios B. Giannakis

**Abstract:** The growing interest towards ultra-wideband (UWB) communications stems from its unique features such as baseband operation, ample multipath diversity, and the potential of enhanced user capacity. But since UWB has to overlay existing narrowband systems, multiple access has to be achieved in the presence of narrowband interference (NBI). However, existing baseband spreading codes for UWB multiple access are not flexible in handling NBI. In this paper, we introduce two novel spreading codes that not only enable baseband UWB multiple access, but also facilitate flexible NBI cancellation. We construct our codes using a single carrier or multiple carriers (SC or MC), which can be implemented with standard discrete-cosine transform (DCT) circuits. With our SC/MC codes, NBI can be avoided by simply nulling undesired digital carriers. Being digital, these SC/MC codes give rise to multi-band UWB systems, without invoking analog carriers. In addition, our SC/MC codes enable full multipath diversity, and maximum coding gains. Equally attractive is their capability to reduce the number of interfering users, with simple matched filter operations. Comprehensive simulations are also carried out to corroborate our analysis.

**Index Terms:** Ultra-wideband (UWB), diversity gain, coding gain, multipath, RAKE, direct-sequence (DS), single-carrier (SC), multi-carrier (MC), narrowband interference (NBI), multi-user interference (MUI), discrete cosine transform (DCT).

## I. INTRODUCTION

With the recent release of the ultra-wideband (UWB) spectral mask by the Federal Communications Commission, UWB has emerged as an exciting technology for commercial wireless communications [1]. Conveying information over ultra-short waveforms, UWB comes with unique features: low-complexity baseband transceivers, ample multipath diversity, and a potential for major increase in user capacity.

To achieve these features, UWB radios have to overlay existing narrowband systems, and be able to accommodate multiple users in the presence of NBI. Existing baseband<sup>1</sup> spreading schemes for multiple access rely on time-hopping (TH),

Manuscript received August 5, 2003.

The authors are with the Department of Electrical and Computer Engineering, University of Minnesota, 200 Union Street, Minneapolis, MN 55455, USA. email: {lqyang,georgios}@ece.umn.edu.

This work was prepared through collaborative participation in the Communications and Networks Consortium sponsored by the U.S. Army Research Laboratory under the Collaborative Technology Alliance Program, Cooperative Agreement DAAD19-01-2-0011. The U.S. Government is authorized to reproduce and distribute reprints for Government purposes notwithstanding any copyright notation thereon. This work was also supported by the NSF Grant No. EIA-0324864. Part of this work was presented at the IEEE Conf. on Ultra-Wideband Systems and Technologies, Reston, VA, Nov. 2003.

<sup>1</sup>Baseband here refers to "carrier-less;" i.e., transmissions free of analog carriers.

or direct-sequence (DS) codes [2]–[4]. These codes can lead to constant-modulus transmissions, but they are not as flexible in handling multi-user interference (MUI) and NBI with low-complexity receivers – two critical factors limiting performance of UWB radios in the presence of multipath and co-existing narrowband services.

As an alternative, we develop here two multi-band UWB multiple access systems that utilize novel digital single-carrier (SC) or multi-carrier (MC) spreading codes. Our SC/MC codes are digital, lead to baseband operation, and offer flexibility in NBI cancellation by simply avoiding carriers residing on the contaminated band. Based on discrete cos/sin functions, these SC/MC codes also enjoy low-complexity implementation with standard discrete cosine transform (DCT) circuits.

Different from orthogonal frequency division multiple access (OFDMA) in narrowband systems [5], our baseband SC- and MC-UWB spreading codes are real. The resulting baseband transceivers are carrier-free and thus immune to carrier frequency offset arising from oscillators' mismatch. Unlike OFDMA that has to resort to channel coding and/or frequency hopping to mitigate frequency-selective fading, we show that UWB signaling even with our single-carrier spreading code occupies multiple frequency bands, and the resulting multi-band transmission enjoys multipath diversity gains. In fact, quantifying performance in terms of diversity order and coding gain, we prove that both SC-UWB and MC-UWB codes enable full multipath diversity, whereas DS-UWB does not. In addition, MC-UWB codes can also enable maximum coding gains. Equally attractive is their capability to mitigate multi-user interference, with simple matched filtering operations.

The rest of this paper is organized as follows. The SC and MC spreading codes are introduced in Section II. Section III introduces a digital model based on RAKE reception in the presence of inter-frame interference, which facilitates performance analysis of DS-, SC-, and MC-UWB systems under a common denominator. In Section IV, the error performance of DS-, SC-, and MC-UWB is quantified in terms of diversity and coding gains. Their performance in multiuser settings is investigated in Section V. Simulations corroborating our analysis are presented in Section VI, and summarizing remarks are given in Section VII.

**Notation:** We will use bold upper (lower) case letters to denote matrices (column vectors) and  $F_N$  to denote a  $N \times N$  FFT matrix. We will use  $I_N$  to represent a  $N \times N$  identity matrix, and  $\mathbf{0}_{M \times N}$  for a  $M$  by  $N$  all zero matrix;  $e_n$  stands for the  $(n + 1)$ st column of an identity matrix. The  $(n + 1)$ st entry of  $\mathbf{a}$  is denoted by  $[\mathbf{a}]_n$ , and the  $(m + 1, n + 1)$ st element of  $\mathbf{A}$  by  $[\mathbf{A}]_{m,n}$ . We will use  $(\cdot)^T$  and  $(\cdot)^H$  for transpose and conjugated transpose,  $\lfloor \cdot \rfloor$  for the floor operation,  $\text{diag}\{\mathbf{a}\}$  for a diagonal

matrix with  $\mathbf{a}$  sitting on the diagonal,  $\det\{\mathbf{A}\}$  and  $\text{tr}\{\mathbf{A}\}$  for the determinant and trace of a matrix  $\mathbf{A}$ , respectively. We will also use  $E\{\cdot\}$  for expectation, and  $:=$  for “is defined as.”

## II. DIGITAL-CARRIER MULTI-BAND USER CODES

Consider a multi-access UWB system with  $N_u$  users, where  $s_u(n_s)$  denotes the  $n_s$ th information bearing symbol of user  $u$ . Every symbol is represented by  $N_f$  ultra-short pulses  $p(t)$  of duration  $T_p$ , transmitted over  $N_f$  frames (one pulse per frame of duration  $T_f$ ). The symbol transmitted during the  $k$ th frame can thus be written as  $s_u(\lfloor k/N_f \rfloor)$ . With symbol duration  $T_s := N_f T_f$ , the symbol rate is  $R := 1/T_s$ . And with  $T_p$  in the order of nanoseconds, the transmission is UWB with bandwidth  $B \approx 1/T_p$ . Using binary pulse amplitude modulation (PAM), the  $u$ th user’s transmitted signal is

$$x_u(t) = \sqrt{\frac{\mathcal{E}_u}{N_f}} \sum_{k=0}^{\infty} s_u(\lfloor k/N_f \rfloor) c_u(k) p(t - kT_f), \quad (1)$$

where  $\mathcal{E}_u$  is the energy per symbol, and  $c_u(k)$  denotes the spreading code of the  $u$ th user,  $\forall u \in [0, N_u - 1]$ . Different from the well known DS codes [2], [3], [6],  $c_u(k)$  here will be SC or MC. Similar to DS though, these new codes will be periodic with period  $N_f$ , and with energy normalized so that  $\sum_{k=0}^{N_f-1} c_u^2(k) = N_f, \forall u \in [0, N_u - 1]$ .

### A. Baseband Single-Carrier UWB

To introduce our SC-UWB user codes, let us first define  $N_u = N_f$  digital carriers  $\forall k \in [0, N_f - 1]$

$$[g_u]_k = \begin{cases} \sqrt{2} \cos(2\pi f_u k), & \text{if } u \in \left[0, \frac{N_f}{2} - 1\right], \\ \sqrt{2} \sin(2\pi f_u k), & \text{if } u \in \left[\frac{N_f}{2}, N_f - 1\right], \end{cases} \quad (2)$$

where  $f_u := (u + 0.5)/N_f, \forall u \in [0, N_f - 1]$ . The SC spreading code during the  $k$ th frame is then given by  $c_u(k) = [g_u]_k$ , which means that the  $u$ th user relies on the *digital* frequency  $f_u$  to spread symbols. Stacking the  $N_f$  carriers into a matrix  $\mathbf{G}_{sc} := [g_0 \cdots g_{N_f-1}]$ , we construct the SC-UWB user codes as

$$\mathbf{c}_u = \mathbf{G}_{sc} \mathbf{e}_u, \quad \forall u \in [0, N_f - 1], \quad (3)$$

where  $\mathbf{c}_u := [c_u(0), \dots, c_u(N_f - 1)]^T$ , and  $\mathbf{e}_n$  denotes the  $(n + 1)$ st column of the identity matrix  $\mathbf{I}_{N_f}$ . It can be easily verified that these digital SC spreading codes are orthogonal:  $\mathbf{c}_{u_1}^T \mathbf{c}_{u_2} = N_f \delta(u_1 - u_2)$ ; hence, the maximum number of users is  $N_u = N_f$ , as in DS-UWB using orthogonal DS sequences.

Different from *narrowband* OFDMA, the codes in (3) are baseband real. More importantly, in *ultra-wideband* operation, these SC spreading codes result in multi-band transmissions. To reveal this *multi-band feature* of SC-UWB, we will next derive the power spectral density (PSD) of  $x_u(t)$  in (1), when the SC codes of (3) are utilized.

For i.i.d. equi-probable binary PAM symbols, the PSD of  $x_u(t)$  in (1) can be expressed as [7, Chapter 4]

$$\Phi_{xx}^{(u)}(f) = \frac{\mathcal{E}_u}{N_f T_s} |P_{s,u}(f)|^2, \quad (4)$$

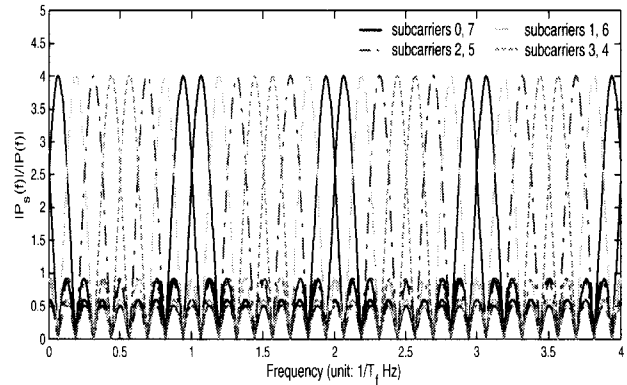


Fig. 1. Subcarriers in baseband SC-UWB ( $N_f = 8, N_p = 4$ ).

where  $P_{s,u}(f) := \mathcal{F}\{p_{s,u}(t)\}$  is the Fourier Transform (FT) of the symbol level pulse shaper  $p_{s,u}(t) := \sum_{k=0}^{N_f-1} c_u(k) p(t - kT_f)$ . With the SC spreading codes in (3), it can be readily verified that

$$P_{s,u}(f) = P(f) \sum_{k=-\infty}^{+\infty} S\left(f - \frac{k}{T_f} - \frac{f_u}{T_f}\right) \pm S\left(f - \frac{k}{T_f} + \frac{f_u}{T_f}\right), \quad (5)$$

where  $P(f) := \mathcal{F}\{p(t)\}$ , and  $S(f) := (T_s/\sqrt{2}) \exp(-j\pi T_s f) \text{sinc}(T_s f)$ , with  $\text{sinc}(f) := \sin(\pi f)/(\pi f)$ . The ‘+’ sign between the two  $S(\cdot)$  terms in (5) corresponds to users  $u \in [0, N_f/2 - 1]$ , while the ‘-’ sign corresponds to users  $u \in [N_f/2, N_f - 1]$ .

The non-zero frequency support of  $P(f)$  is inversely proportional to the pulse duration  $T_p$ ; whereas the sinc function has main lobe width  $(2/T_s)$  Hz, and is repeated every  $(1/T_f)$  Hz. Letting  $N_p := T_f/T_p$  be an integer without loss of generality, we deduce that there are  $2N_p$  sinc main lobes over the bandwidth of  $P(f)$ . In UWB transmissions that typically have low duty-cycle,  $T_f \gg T_p$  implies that the number of sinc main lobes  $2N_p \gg 2$ . In other words, utilizing a single digital “carrier”  $f_u$ , each user’s transmission occupies multiple frequency bands, as depicted in Fig. 1. Also notice that since we introduced a  $0.5/N_f$  shift in the definition of  $f_u$  in (2), each user (subcarrier) occupies the same bandwidth.

The multi-band feature of SC-UWB implies that each user’s transmission is spread over the ultra-wide bandwidth, and enjoys the associated multipath diversity gains. In fact, we will later prove that our baseband real SC-UWB codes in (3) enable full multipath diversity, in contrast with narrowband OFDMA systems that have to resort to channel coding and/or frequency hopping to mitigate frequency-selective fading at the expense of (possibly considerable) bandwidth overexpansion.

Also implied by Fig. 1 is the flexibility offered by SC-UWB in handling (e.g., GPS or WLAN induced) NBI. Since the transmit spectrum is distinctly determined by the digital carrier  $f_u$ , one gains resilience to NBI by simply avoiding usage of carriers residing on (or close to) these services. Such a flexibility in NBI avoidance is also shared by the MC-UWB spreading codes that we introduce next.

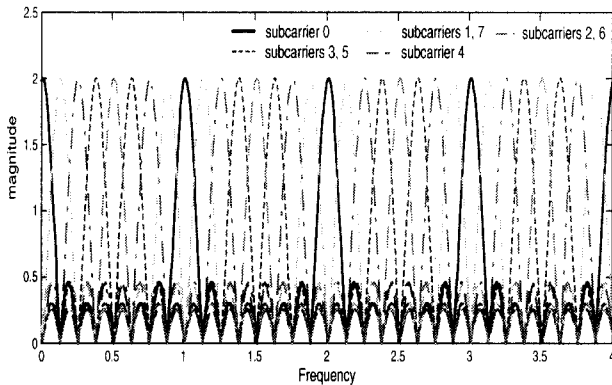


Fig. 2. Subcarriers in baseband MC-UWB ( $N_f = 8$ ,  $N_p = 4$ ).

### B. Baseband Multi-Carrier UWB

Instead of a single carrier, in multi-carrier (MC)-UWB, each user can utilize all digital carriers. To construct  $N_u (= N_f)$  such user-specific codes  $c_u(k)$ , let us first define the following  $N_f \times 1$  digital carriers  $\forall k \in [0, N_f - 1]$

$$[\bar{g}_n]_k = \begin{cases} \cos(2\pi f_n k), & n = 0, \text{ or } n = \frac{N_f}{2} \\ \sqrt{2} \cos(2\pi f_n k), & n \in [1, \frac{N_f}{2} - 1] \\ \sqrt{2} \sin(2\pi f_n k), & n \in [\frac{N_f}{2} + 1, N_f - 1] \end{cases}, \quad (6)$$

where  $f_n := n/N_f$ . Stacking the  $N_f$  carriers into a matrix  $\mathbf{G}_{mc} := [\bar{g}_0 \cdots \bar{g}_{N_f-1}]$ , we construct the MC-UWB spreading codes as

$$c_u = \mathbf{G}_{mc} c_u^{(o)}, \quad \forall u \in [0, N_f - 1], \quad (7)$$

where  $\{c_u^{(o)}\}_{u=0}^{N_f-1}$  denote any set of real orthonormal sequences (each of length  $N_f$ ). Evidently, the resultant MC codes are also orthogonal.

Similar to SC-UWB, the digital carriers (6) also give rise to multi-band transmissions with multiple sinc main lobes within the frequency support of  $P(f)$ . This multi-band feature of MC-UWB is illustrated by the discrete-time Fourier Transform (DTFT) of  $\bar{g}_k$ 's in Fig. 2. Also similar to SC-UWB, each MC carrier has a distinct frequency support, which enables flexible NBI suppression by simply avoiding contaminated carriers.

Though similar, the SC and MC codes are designed differently and have distinct merits. Comparing the digital SC and MC codes, we notice that the shift of  $0.5/N_f$  in  $f_u$  is present in (2), but not in (6). The difference becomes evident when comparing Figs. 1 and 2: chosen for SC-UWB as in (2), each digital carrier corresponds to the same number of sinc main lobes ( $2N_p = 8$  in Fig. 1); whereas chosen for MC-UWB as in (6), the 0th and the 4th carriers each contains only half as many sinc main lobes as other carriers (see Fig. 2). Consequently, specializing (6) to SC (by setting  $c_u^{(o)} = e_u$ ) transmissions will induce unbalanced user bandwidth, which we will show to imply user-dependent multipath diversity. But since MC-UWB allows each user to utilize *all* carriers with the MC codes in (7), there is no need to equate the bandwidth of each carrier. This explains why the  $0.5/N_f$  shift is not included in  $f_n$  for the MC spreading codes in (6).

Despite their differences, SC/MC codes share one attractive feature: they both facilitate low-complexity implementation using standard DCT circuits, thanks to their construction based on discrete cos/sin functions. This implementation advantage also distinguishes them from the analog SC-UWB codes introduced in [8] that aim to offer robustness against user asynchronism. Also different from the WirelessPAN multi-band proposals that rely on analog carriers, our SC/MC codes achieve multi-band transmission using baseband operations. Compared to analog multi-band solutions that entail multiple local oscillators, our carrier-free multi-band SC/MC-UWB not only enjoys low-complexity implementation, but are also exempt from carrier frequency offsets that are known to degrade performance (of e.g., OFDMA) severely.

So far, we have introduced our baseband real SC/MC codes, their construction, and the resultant multi-band transmissions. To facilitate performance analysis of our SC/MC-UWB, and reveal their merits with respect to existing DS-UWB alternatives, we need to establish the system's input-output (I/O) relationship in digital form.

### III. FRAME-RATE SAMPLED MODEL WITH RAKE RECEPTION

In this section, we will derive the baseband digital model of a multi-access UWB system with RAKE reception. To reach the receiver, the  $u$ th user's transmission propagates through a (dense) multipath channel with impulse response:  $\sum_{l=0}^{L_u} \alpha_u(l) \delta(t - \tau_u(l))$ , where  $\{\alpha_u(l)\}_{l=0}^{L_u}$  and  $\{\tau_u(l)\}_{l=0}^{L_u}$  are amplitudes and delays corresponding to a total of  $L_u$  multipath returns. The continuous-time received waveform is then given by [c.f. (1)]

$$r(t) = \sum_{u=0}^{N_u-1} \sqrt{\frac{\mathcal{E}_u}{N_f}} \cdot \sum_{k=0}^{\infty} s_u \left( \left\lfloor \frac{k}{N_f} \right\rfloor \right) \cdot c_u(k) h_u(t - kT_f) + \eta(t), \quad (8)$$

where  $h_u(t) := \sum_{l=0}^{L_u} \alpha_u(l) p(t - \tau_u(l))$  is the composite "pulse-multipath" channel corresponding to user  $u$ , and  $\eta(t)$  is the aggregate noise including additive white Gaussian noise (AWGN), and possible NBI. Notice that after multipath propagation, each UWB pulse  $p(t)$  is time-dispersed to the waveform  $h_u(t)$  of duration  $\tau_u(L_u) + T_p$ . To allow for high data-rates, the frame duration is chosen to satisfy:  $T_f < \tau_u(L_u) + T_p$ , which induces inter-frame interference (IFI).

After the channel has been estimated, RAKE reception is often adopted to collect the ample multipath diversity provided by UWB channels [9]. RAKE receivers with  $L$  fingers sum up weighted outputs (diversity combining) from a bank of  $L$  correlators. Let  $\{\tau(l)\}_{l=1}^L$  denote the delays corresponding to the total of  $L$  RAKE fingers, sorted in an increasing manner (notice that the RAKE delays  $\tau(l)$  are not necessarily equal to the channel delays  $\tau_u(l)$ ). To collect energy from all fingers, the maximum delay  $\tau(L)$  must not exceed the multipath delay spread. Furthermore, to collect samples at frame rate,  $\tau(L)$  is also confined by the frame duration  $T_f$ . As a result,

the maximum RAKE finger delay is upper bounded by:  $\tau(L) \leq \min\{T_f - T_p, \tau_\mu(L_\mu) + T_p\}$ , where  $\mu$  here denotes the desired user. We do not otherwise impose any constraints on RAKE fingers. In practice,  $L$  and  $\{\tau(l)\}_{l=1}^L$  can be either channel-dependent or fixed depending on error performance versus complexity tradeoffs. These tradeoffs lead to various choices: all-RAKE, partial-RAKE, or selective-RAKE receivers [10].

During the  $k$ th frame, the correlator template for the  $l$ th RAKE finger is the pulse  $p(t - kT_f - \tau(l))$ . Accordingly, the correlator output is  $y(k; l) := \int_{kT_f + \tau(l)}^{kT_f + \tau(l) + T_p} r(t)p(t - kT_f - \tau(l))dt$ . Denoting the correlation between the template waveform  $p(t)$  and the received waveform  $h_u(t)$  as  $\rho_{u,h}(\tau) := \int_{\tau}^{\tau + T_p} p(t - \tau)h_u(t)dt$ , the correlator output can be re-expressed as  $y(k; l) = \sum_{u=0}^{N_u-1} \sqrt{\frac{\mathcal{E}_u}{N_f}} \sum_{n=0}^{\infty} s_u(\lfloor n/N_f \rfloor) c_u(n) \rho_{u,h}((k - n)T_f + \tau(l) + \eta(k; l))$ , where  $\eta(k; l)$  denotes the corresponding sampled noise. To simplify this expression, let us define  $\alpha_{u,l}(n) := \rho_{u,h}(nT_f + \tau(l))$ . The resultant correlator output of the  $l$ th finger during the  $k$ th frame is

$$y(k; l) = \sum_{u=0}^{N_u-1} \sqrt{\frac{\mathcal{E}_u}{N_f}} \sum_{n=0}^{+\infty} \alpha_{u,l}(n) c_u(k - n) s_u \left( \left\lfloor \frac{k - n}{N_f} \right\rfloor \right) + \eta(k; l), \quad \forall l \in [1, L]. \quad (9)$$

Equation (9) represents the I/O relationship of our frame-sampled discrete-time equivalent pulse-multipath-RAKE system model. Using the definition of  $\rho_{u,h}(\tau)$ , it can be readily verified that: i) cascading the RAKE with the pulse-multipath channel yields a discrete-time equivalent channel with taps  $\{\alpha_{u,l}(n)\}$  corresponding to user  $u$  per finger  $l$ ; and ii) the summation over  $n$  captures the IFI.

Seemingly infinite, the number of IFI-inducing frames in (9) is actually finite. This is because the discrete-time equivalent channel is of finite length, as the underlying physical channel is (at least approximately). Indeed, for any  $u$  and  $l$ , we have  $\alpha_{u,l}(n) = 0$ , if  $nT_f + \tau(l) \geq \tau_u(L_u) + T_p$ . Therefore, the discrete-time equivalent channel  $\{\alpha_{u,l}(n)\}_{n=0}^{M_{u,l}}$  corresponding to user  $u$  per finger  $l$  has order

$$M_{u,l} := \max\{n : \tau(l) + nT_f < \tau_u(L_u) + T_p\}. \quad (10)$$

Accordingly, (9) boils down to

$$y(k; l) = \sum_{u=0}^{N_u-1} \sqrt{\frac{\mathcal{E}_u}{N_f}} \sum_{n=0}^{M_{u,l}} \alpha_{u,l}(n) c_u(k - n) s_u \left( \left\lfloor \frac{k - n}{N_f} \right\rfloor \right) + \eta(k; l), \quad \forall l \in [1, L]. \quad (11)$$

Notice that IFI is present, as long as the maximum channel order  $\max_{u,l}\{M_{u,l}\} > 0$ . If we select  $T_f \geq \max_u\{\tau_u(L_u)\} + T_p - \tau(1)$ , then  $M_{u,l} = 0$ ,  $\forall u, l$ , and IFI vanishes. When IFI involves more than one symbol, inter-symbol interference (ISI) emerges on top of IFI. It can be verified though, that ISI is confined to two consecutive symbols, as long as  $\max_u\{\tau_u(L_u)\} + T_p - \tau(1) \leq T_s$ . The latter is satisfied in a low power, low duty-cycle UWB system, because  $T_s = N_f N_p T_p$  is generally much greater than the channel's maximum delay spread (30 ~ 100ns). For notational simplicity, we assume that this condition is satisfied. But it is worth mentioning that our analysis hereafter can be generalized to cases where this condition is not satisfied.

Let us now stack correlator outputs corresponding to the same finger  $l$  from the frames conveying the  $n_s$ th symbol, to form the block  $\mathbf{y}(n_s; l) := [y(n_s N_f; l), \dots, y(n_s N_f + N_f - 1; l)]^T$ . The following I/O relationship can then be obtained from (11)

$$\mathbf{y}(n_s; l) = \sum_{u=0}^{N_u-1} \sqrt{\frac{\mathcal{E}_u}{N_f}} \mathbf{H}_{u,l}^{(0)} \mathbf{c}_u s_u(n_s) + \sum_{u=0}^{N_u-1} \sqrt{\frac{\mathcal{E}_u}{N_f}} \mathbf{H}_{u,l}^{(1)} \mathbf{c}_u s_u(n_s - 1) + \boldsymbol{\eta}(n_s; l), \quad (12)$$

where  $\boldsymbol{\eta}(n_s; l) := [\eta(n_s N_f; l), \dots, \eta(n_s N_f + N_f - 1; l)]^T$ ,  $\mathbf{H}_{u,l}^{(0)}$  is a  $N_f \times N_f$  lower triangular Toeplitz matrix with first column  $[\alpha_{u,l}(0), \dots, \alpha_{u,l}(M_{u,l}), 0, \dots, 0]^T$ , and  $\mathbf{H}_{u,l}^{(1)}$  is a  $N_f \times N_f$  upper triangular Toeplitz matrix with first row  $[0, \dots, 0, \alpha_{u,l}(M_{u,l}), \dots, \alpha_{u,l}(1)]$ .

To collect all the information related to the  $n_s$ th symbol, we concatenate vectors  $\{\mathbf{y}(n_s; l)\}_{l=1}^L$  from all RAKE fingers into a super vector  $\mathbf{y}(n_s) := [\mathbf{y}^T(n_s; 1), \dots, \mathbf{y}^T(n_s; L)]^T$  of size  $N_f L \times 1$  which can be expressed as [c.f. (12)]

$$\mathbf{y}(n_s) = \sum_{u=0}^{N_u-1} \sqrt{\frac{\mathcal{E}_u}{N_f}} \mathbf{H}_u^{(0)} \boldsymbol{\nu}_u(n_s) + \sum_{u=0}^{N_u-1} \sqrt{\frac{\mathcal{E}_u}{N_f}} \mathbf{H}_u^{(1)} \boldsymbol{\nu}_u(n_s - 1) + \boldsymbol{\eta}(n_s), \quad (13)$$

where the  $N_f \times 1$  block  $\boldsymbol{\nu}_u(n) := \mathbf{c}_u s_u(n)$  is the  $n$ th symbol spread over  $N_f$  frames,  $\boldsymbol{\eta}(n_s) := [\boldsymbol{\eta}^T(n_s; 1), \dots, \boldsymbol{\eta}^T(n_s; L)]^T$  is the  $N_f L \times 1$  noise vector associated with the  $n_s$ th symbol, and  $\mathbf{H}_u^{(0)} := [\mathbf{H}_{u,1}^{(0)T}, \dots, \mathbf{H}_{u,L}^{(0)T}]^T$  and  $\mathbf{H}_u^{(1)} := [\mathbf{H}_{u,1}^{(1)T}, \dots, \mathbf{H}_{u,L}^{(1)T}]^T$ . Notice that the ISI (second sum in (12)) has given rise to an inter-block interference (IBI) term (second term in (13)).

Targeting block by block detection, IBI (and thus ISI) needs to be removed. From the definition of  $M_{u,l}$  in (10), it follows that the maximum discrete-time equivalent channel order is  $M_1 = \max_{u,l}\{M_{u,l}\}$ . Consequently, padding each block  $\boldsymbol{\nu}_u(n)$  with  $M_1$  zero-guards allows the channel to settle down before the next block/symbol arrives, and thus eliminates the IBI terms of all users. Zero-padding (ZP) each block  $\boldsymbol{\nu}_u(n)$  with  $M_1$  trailing zeros prior to transmission, the I/O relationship in (13) simplifies to an IBI-free one

$$\mathbf{y}_{zp} = \sum_{u=0}^{N_u-1} \sqrt{\frac{\mathcal{E}_u}{N_f}} \bar{\mathbf{H}}_u \boldsymbol{\nu}_u + \boldsymbol{\eta}, \quad (14)$$

where the index  $n_s$  is dropped for notational simplicity, and  $\bar{\mathbf{H}}_u := [\bar{\mathbf{H}}_{u,1}^T, \dots, \bar{\mathbf{H}}_{u,L}^T]^T$  is the  $LN_1 \times N_f$  channel matrix with  $N_1 := N_f + M_1$ . The  $l$ th block of the channel matrix  $\bar{\mathbf{H}}_{u,l}^T$  is a  $N_1 \times N_f$  lower triangular Toeplitz matrix with the first column given by  $[\alpha_{u,l}(0), \dots, \alpha_{u,l}(M_{u,l}), 0, \dots, 0]^T$ .

Instead of having  $M_1$  zeros padded at the end of each block  $\boldsymbol{\nu}_u$ , an alternative way to eliminate IBI is by adding a cyclic prefix (CP) of length  $M_1$  at the transmitter and removing it at the receiver, much like OFDMA. Intuitively, since only the first  $M_1$

elements per block are contaminated by IBI, we can introduce redundancy at the transmission and discard it upon reception. In this case, the I/O relationship becomes

$$\mathbf{y}_{cp} = \sum_{u=0}^{N_u-1} \sqrt{\frac{\mathcal{E}_u}{N_f}} \tilde{\mathbf{H}}_u \boldsymbol{\nu}_u + \boldsymbol{\eta}, \quad (15)$$

where now the channel matrix is  $\tilde{\mathbf{H}}_u := [\tilde{\mathbf{H}}_{u,1}^T, \dots, \tilde{\mathbf{H}}_{u,L}^T]^T$ . By inserting and removing CP, each block of the channel matrix  $\tilde{\mathbf{H}}_{u,l}^T$  becomes a  $N_f \times N_f$  column-wise circulant matrix with the first column given by  $[\alpha_{u,l}(0), \dots, \alpha_{u,l}(M_{u,l}), 0, \dots, 0]^T$  (c.f. Toeplitz in (14)).

Although *continuous-time* and *over-sampled* RAKE receiver models are well-documented in the UWB literature (e.g., [9], [10], [11]), (14) and (15) are novel and interesting because they describe in a *discrete-time frame-rate* sampled form the aggregate pulse-multipath-RAKE model in the presence of IFI. Eqs. (14) and (15) also show that frame-by-frame RAKE correlator samples obey a matrix-vector I/O relationship free of IBI (ISI) even in dense multipath channels, provided that suitable guards (zero-padding or cyclic prefix) are inserted in UWB transmissions. These expressions are surprisingly simple if one takes into account that they include IFI effects that are always present in high-rate UWB radios. Based on (14) and (15), we will benchmark the performance of UWB spreading codes in Section IV, and investigate their error performance in a multi-user scenario in Section V.

#### IV. PERFORMANCE ANALYSIS

In this section, we will assess the performance corresponding to different spreading codes by quantifying their diversity and coding gains in the presence of UWB multipath. This will allow comparisons of our novel spreading codes relative to existing DS ones in the presence of IFI. To quantify diversity and coding gains for a particular user, we set  $N_u = 1$ . We also suppose  $\{\alpha_{u,l}\}_{l=1}^L := [\alpha_{u,l}(0), \dots, \alpha_{u,l}(M_{u,l})]^T$  are perfectly known at the receiver, to isolate these effects from channel estimation imperfections.

Let us consider the pairwise error probability (PEP)  $P(\boldsymbol{\nu}_u \rightarrow \boldsymbol{\nu}'_u | \{\alpha_{u,l}\}_{l=1}^L)$  of erroneously decoding  $\boldsymbol{\nu}_u$  as  $\boldsymbol{\nu}'_u \neq \boldsymbol{\nu}_u$ , assuming a maximum likelihood (ML) detector. The PEP can be upper bounded at high SNR using the Chernoff bound

$$P(\boldsymbol{\nu}_u \rightarrow \boldsymbol{\nu}'_u | \{\alpha_{u,l}\}_{l=1}^L) \leq \exp\left(\frac{-d^2(\bar{\mathbf{y}}, \bar{\mathbf{y}}')}{4N_0}\right), \quad (16)$$

where  $N_0/2$  is the noise variance, and  $\bar{\mathbf{y}}$  ( $\bar{\mathbf{y}}'$ ) is the noise-free part of (14) [or (15)], corresponding to  $\boldsymbol{\nu}_u$  ( $\boldsymbol{\nu}'_u$ ), and  $d(\bar{\mathbf{y}}, \bar{\mathbf{y}}') := \|\bar{\mathbf{y}} - \bar{\mathbf{y}}'\|$  is the Euclidean distance between them. Using (14) and (15), we have

$$d^2(\bar{\mathbf{y}}, \bar{\mathbf{y}}') = \frac{\mathcal{E}_u}{N_f} \epsilon^2 \mathbf{c}_u^T \mathbf{H}_u^T \mathbf{H}_u \mathbf{c}_u, \quad (17)$$

where  $\epsilon := s_u - s'_u$ ,  $\mathbf{H}_u = \tilde{\mathbf{H}}_u$  with ZP guards, and  $\mathbf{H}_u = \tilde{\mathbf{H}}_u$  with CP guards. Eq. (17) implies that for each given channel realization, the PEP depends on the spreading

code  $\mathbf{c}_u$ . We will show next how different spreading codes (DS, SC, or MC) affect the average PEP  $P(\boldsymbol{\nu}_u \rightarrow \boldsymbol{\nu}'_u) := E_{\boldsymbol{\alpha}} \{P(\boldsymbol{\nu}_u \rightarrow \boldsymbol{\nu}'_u | \{\alpha_{u,l}\}_{l=1}^L)\}$ .

Denoting the pair-wise error as  $\epsilon_u := \boldsymbol{\nu}_u - \boldsymbol{\nu}'_u$ , we show in Appendix I that (16) can be re-expressed as

$$P(\boldsymbol{\nu}_u \rightarrow \boldsymbol{\nu}'_u | \{\alpha_{u,l}\}_{l=1}^L) \leq \exp\left(\frac{-\mathcal{E}_u \sum_{l=1}^L \boldsymbol{\alpha}_{u,l}^T \boldsymbol{\Theta}_{\epsilon_u}^{(u,l)} \boldsymbol{\alpha}_{u,l}}{4N_f N_0}\right), \quad (18)$$

where  $\boldsymbol{\Theta}_{\epsilon_u}^{(u,l)} := \mathbf{E}_{u,l}^T \mathbf{E}_{u,l}$  in the ZP case, with  $\mathbf{E}_{u,l}$  being a  $N_f \times (M_{u,l} + 1)$  Toeplitz matrix with first column  $[\epsilon_u(0), \dots, \epsilon_u(N_f - 1), 0, \dots, 0]^T$ . With CP guards,  $\boldsymbol{\Theta}_{\epsilon_u}^{(u,l)} = N_f \mathbf{F}_{0:M_{u,l}}^H \mathbf{D}_{\epsilon_u}^H \mathbf{D}_{\epsilon_u} \mathbf{F}_{0:M_{u,l}}$ , where  $\mathbf{F}_{0:m}$  denotes the matrix formed by the first  $(m + 1)$  columns of  $\mathbf{F}_{N_f}$ , and  $\mathbf{D}_{\epsilon_u} := \text{diag}\{\epsilon_u\}$  with  $\epsilon_u := \mathbf{F}_{N_f} \epsilon_u$ .

Let  $r_{\epsilon_u}^{(u,l)}$  denote the rank of  $\boldsymbol{\Theta}_{\epsilon_u}^{(u,l)}$ , and  $\{\lambda_{\epsilon_u}^{(u,l)}(m)\}_{m=0}^{M_{u,l}}$  denote its nonincreasing eigenvalues. Supposing the entries of  $\alpha_{u,l}(n)$  are zero-mean, uncorrelated Gaussian, with variance  $\mathcal{A}_{u,l}(n) = E\{\alpha_{u,l}^2(n)\}$ , we show in Appendix II that at high SNR ( $\mathcal{E}_u/N_0 \gg 1$ ), the average PEP is upper bounded by

$$P(\boldsymbol{\nu}_u \rightarrow \boldsymbol{\nu}'_u) \leq \left(\frac{\mathcal{E}_u}{2N_0} G_{c,\epsilon}\right)^{-G_{d,\epsilon}}, \quad (19)$$

where  $G_{d,\epsilon} := (1/2) \sum_{l=1}^L r_{\epsilon_u}^{(u,l)}$  denotes the diversity gain, and  $G_{c,\epsilon} := \left[\prod_{l=1}^L \prod_{m=0}^{r_{\epsilon_u}^{(u,l)}-1} \frac{\mathcal{A}_{u,l}(m) \lambda_{\epsilon_u}^{(u,l)}(m)}{N_f}\right]^{1/(2G_{d,\epsilon})}$  the coding gain for the error vector  $\epsilon_u$ . Eq. (19) reveals that at high SNR, the average PEP is uniquely characterized by two parameters: the diversity gain  $G_{d,\epsilon}$  determining the PEP slope as a function of log-SNR, and the coding gain  $G_{c,\epsilon}$  determining its shift. As  $\boldsymbol{\Theta}_{\epsilon_u}^{(u,l)}$  is directly related to  $\mathbf{c}_u$ , the average PEP depends on spreading code used. Interestingly, if  $\alpha_{u,l}(m)$ 's are uncorrelated complex Gaussian with variance  $\mathcal{A}_{u,l}(m)/2$  per real dimension (see e.g., [12]), then  $G_{d,\epsilon}$  will be doubled, whereas  $G_{c,\epsilon}$  will be halved.

Both  $G_{d,\epsilon}$  and  $G_{c,\epsilon}$  depend on  $\epsilon_u$ . Accounting for all possible pairwise errors, we define the diversity order and coding gains as  $G_d := \min_{\epsilon_u \neq \mathbf{0}} \{G_{d,\epsilon}\}$ , and  $G_c := \min_{\epsilon_u \neq \mathbf{0}} \{G_{c,\epsilon}\}$ , respectively. Subject to the underlying physical channel and the UWB system parameters, we will subsequently upper bound these diversity and coding gains. To this end, we assume that the physical channel taps are zero-mean uncorrelated Gaussian, and establish first the following lemma<sup>2</sup>:

**Lemma 1:** In a UWB system with parameters  $N_f$ ,  $T_f$ , and  $T_p$ , and  $L$ -finger RAKE reception with  $L \leq L_u$  and delays  $\{\tau(l)\}_{l=1}^L$  spaced at least  $2T_p$  apart, the following hold:

1) With the equivalent channel order  $M_{u,l}$  as in (10), the max-

<sup>2</sup>In fact, the proof of Lemma 1 shows that full diversity only requires  $\boldsymbol{\Theta}_{\epsilon_u}^{(u,l)}$  to be full rank,  $\forall l \in [1, L]$ . Therefore, Lemma 1 can be generalized even to correlated channel vectors so long as the correlation matrix is of full rank. In addition, using the results of [13], it can be shown that our diversity and coding gain results apply to all non-Gaussian fading PDFs encountered in practice.

imum achievable diversity order is

$$G_{d,max} = \frac{1}{2} \sum_{l=1}^L (M_{u,l} + 1), \quad (20)$$

and can be guaranteed if and only if  $\Theta_{\varepsilon_u}^{(u,l)}$  is full rank,  $\forall l \in [1, L]$ , and  $\forall \varepsilon_u \neq \mathbf{0}$ .

- 2) With maximum diversity gain  $G_{d,max}$  being achieved, the maximum coding gain is

$$G_{c,max} := d_{min}^2 \left[ \prod_{l=1}^L \prod_{m=0}^{M_{u,l}} \mathcal{A}_{u,l}(m) \right]^{1/(2G_{d,max})}, \quad (21)$$

where  $\mathcal{A}_{u,l}(m) := \mathbb{E}\{\alpha_{u,l}^2(m)\}$ , and  $d_{min}$  is the minimum Euclidean distance of the  $s_u$  constellation. Furthermore,  $G_{c,max}$  can be achieved if and only if  $\Theta_{\varepsilon_u}^{(u,l)}$  is the scaled identity matrix  $N_f(s_u - s'_u)^2 \mathbf{I}_{M_{u,l}+1}$ .

*Proof:* See Appendix III.  $\square$

Notice that Lemma 1 provides *upper bounds* on the achievable diversity order and coding gain. Although dependent on the underlying physical channel and system parameters, the results in (20) and (21) apply to all UWB systems with RAKE reception, irrespective of the underlying spreading code. Intuitively, Lemma 1 asserts that for each (say, the  $l$ th) RAKE finger,  $(M_{u,l} + 1)$  taps of its corresponding discrete-time equivalent channel contribute a maximum diversity order of  $(M_{u,l} + 1)/2$ , where the factor  $1/2$  appears because UWB transmissions are real. Summing up the diversity collected by all fingers  $l \in [1, L]$ , we obtain the maximum diversity order as in (20). With this in mind, the coding gain is nothing but the average SNR gain due to the energy collected from a total of  $\sum_{l=1}^L (M_{u,l} + 1)$  multipath returns. Certainly, the concepts of diversity and coding gains in Lemma 1 are common to any fading channel. But expressions (20) and (21) are tailored for UWB systems with RAKE reception.

**Corollary 1:** If on top of the conditions in Lemma 1, we also select  $T_f \geq \tau_u(L_u) + T_p - \tau(1)$  to remove IFI, the resulting maximum diversity and coding gains are  $G_{d,max} = L/2$ , and  $G_{c,max} = d_{min}^2 [\prod_{l=1}^L \mathcal{A}_{u,l}(0)]^{1/(2G_{d,max})}$ , respectively.

*Proof:* With this additional condition on the frame duration, IFI vanishes; i.e., the discrete-time equivalent channels have orders  $M_{u,l} = 0$ ,  $\forall l \in [1, L]$ . The resultant  $\Theta_{\varepsilon_u}^{(u,l)} = N_f(s_u - s'_u)^2$  becomes a constant, regardless of the spreading code  $c_u$ . The results then follow directly from Lemma 1.  $\square$

It is worth noticing that for a given number of fingers  $L$ , non-zero IFI works to our favor by boosting diversity gains [c.f. (20)], which is intuitively appealing since we collect more energy. Of course, in the absence of IFI, one can increase the number of RAKE fingers  $L$  per frame, which will increase diversity at the expense of increasing complexity and reducing transmission rates (since  $T_f$  must be increased accordingly). As a special case, Corollary 1 quantifies this diversity in the absence of IFI, where as expected,  $G_{d,max}$  is proportional to the number of RAKE fingers  $L$ . In the absence of MUI and NBI, these gains can be collected with maximum ratio combining (MRC) [14].

Having benchmarked the maximum possible diversity and coding gains, and having established conditions for achieving them, we are now ready to compare the gains enabled by DS, SC, and MC spreading codes, with ZP or CP guards.

#### A. With ZP Guards

When IBI is removed with ZP,  $\Theta_{\varepsilon_u}^{(u,l)} = \mathbf{E}_{u,l}^T \mathbf{E}_{u,l}$ . Because  $\{\mathbf{E}_{u,l}\}_{l=1}^L$  in (30) are Toeplitz matrices that guarantee full column rank  $\forall \varepsilon_u \neq \mathbf{0}$ ,  $\Theta_{\varepsilon_u}^{(u,l)}$  has full rank  $r_{\varepsilon_u}^{(u,l)} = M_{u,l} + 1$ ,  $\forall l \in [1, L]$ . Therefore, *regardless of the spreading code used*, the maximum achievable diversity order is always guaranteed:  $G_{d,zp} = G_{d,max}$ ; i.e.,

**Proposition 1:** In a UWB system with parameters  $N_f$ ,  $T_f$ , and  $T_p$ , and  $L$ -finger RAKE reception with delays  $\{\tau(l)\}_{l=1}^L$  spaced at least  $2T_p$  apart, IBI removal with ZP enables the maximum achievable diversity order  $G_{d,zp} = G_{d,max}$ , regardless of the spreading codes used.

Having the same diversity order, the relative error performance of DS-, SC-, and MC-UWB is dictated by their corresponding coding gains. To achieve maximum coding gain, however, requires the spreading codes to have perfect correlation; i.e.,  $\sum_{k=0}^{N_f-1} c_u(k)c_u(k+l) = N_f\delta(l)$ . Generally, this is not guaranteed. But interestingly, our simulations will illustrate that MC-UWB with Walsh-Hadamard  $c_u^{(o)}$  approaches  $G_{c,max}$ ,  $\forall u$ .

#### B. With CP Guards

In the CP case, we have  $\Theta_{\varepsilon_u}^{(u,l)} = N_f \mathbf{F}_{0:M_{u,l}}^H \mathbf{D}_{\varepsilon_u}^H \mathbf{D}_{\varepsilon_u} \mathbf{F}_{0:M_{u,l}}$  and with  $\mathbf{F}_{0:M_{u,l}}$  having full column rank, the rank of  $\Theta_{\varepsilon_u}^{(u,l)}$  is  $r_{\varepsilon_u}^{(u,l)} = \min\{\mathcal{D}_u, M_{u,l} + 1\}$ , where  $\mathcal{D}_u$  is the number of non-zero entries of  $\varepsilon_u$ . To guarantee  $G_{d,max}$  for any  $M_{u,l}$ , all entries of  $\varepsilon_u$  must be non-zero. It can also be verified that to further guarantee  $G_{c,max}$ , the entries of  $\varepsilon_u$  must have identical magnitudes.

Now let us consider whether and under what conditions our SC/MC-UWB codes with CP guards can enable the benchmark diversity and coding gains established by Lemma 1.

For DS-UWB, we have  $\varepsilon_u = (s_u - s'_u) \mathbf{F}_{N_f} c_u$  by definition. With  $c_u(k) \in \{\pm 1\}$ , it can not be guaranteed that all entries of  $\varepsilon_u$  are nonzero. Enabling  $G_{d,max}$  is therefore not guaranteed either. In fact, if Walsh-Hadamard codes are used, it can be shown that the *diversity order is user dependent*

$$G_{d,cp}^{(ds)}(u) = \begin{cases} \frac{1}{2} \sum_{l=1}^L \min\{1, M_{u,l} + 1\} = \frac{L}{2}, & \text{if } u = 0, 1, \\ \frac{1}{2} \sum_{l=1}^L \min\{2^{\lceil \log_2 u \rceil}, M_{u,l} + 1\} \leq G_{d,max}, & \text{otherwise.} \end{cases} \quad (22)$$

For SC-UWB with carriers as in (2), the entries of  $\varepsilon_u$  can be

found  $\forall n \in [0, N_f - 1]$  to be

$$[\epsilon_u]_n = \sqrt{\frac{2}{N_f}}(s_u - s'_u) \times \begin{cases} j \frac{\sin(2\pi n/N_f)}{\cos(2\pi n/N_f) - \cos(2\pi(u+0.5)/N_f)} + 1, & \text{if } u \in [0, N_f/2 - 1], \\ \frac{\sin(2\pi(u+0.5)/N_f)}{\cos(2\pi n/N_f) - \cos(2\pi(u+0.5)/N_f)}, & \text{if } u \in [N_f/2, N_f - 1]. \end{cases} \quad (23)$$

It is clear from (23) that  $\epsilon_u$  will have non-zero entries, for all non-zero errors. As a result, SC-UWB guarantees  $G_{d,cp}^{(sc)} = G_{d,max}$  even with CP guards.

For MC-UWB with carriers as in (6), we have  $\epsilon_u = (s_u - s'_u) \mathbf{F}_{N_f} \mathbf{G}_{mc} \mathbf{c}_u^{(o)}$ . And its  $n$ th element is

$$[\epsilon_u]_n = (s_u - s'_u) \times \begin{cases} \sqrt{N_f} [c_u^{(o)}]_n, & n = 0, \text{ or, } n = \frac{N_f}{2}, \\ \sqrt{N_f/2} \left( [c_u^{(o)}]_n + j [c_u^{(o)}]_{N_f-n} \right), & n \in \left[ 1, \frac{N_f}{2} - 1 \right], \\ \sqrt{N_f/2} \left( [c_u^{(o)}]_{N_f-n} - j [c_u^{(o)}]_n \right), & n \in \left[ \frac{N_f}{2} + 1, N_f - 1 \right]. \end{cases} \quad (24)$$

Equation (24) implies that  $\epsilon_u$  does not contain any zero entry, for all non-zero errors, if and only if the real orthonormal codes  $\mathbf{c}_u^{(o)}$  satisfy the following conditions

$$[c_u^{(o)}]_n + j [c_u^{(o)}]_{\text{mod}(N_f-n, N_f)} \neq 0, \forall n \in [0, N_f - 1], \quad (25)$$

or equivalently, at least one of the two real numbers  $[c_u^{(o)}]_n$  and  $[c_u^{(o)}]_{\text{mod}(N_f-n, N_f)}$  is non-zero. This implies that MC-UWB achieves maximum diversity order  $G_{d,cp}^{(mc)} = G_{d,max}$ , even with CP, if and only if (25) is satisfied. Intuitively speaking, when (25) is satisfied, the resultant  $\epsilon_u$  will give rise to a transmit spectrum that covers the entire bandwidth, and thus enables the maximum multipath diversity provided by the UWB channel. To gain more insight, let us consider two special choices of  $\mathbf{c}_u^{(o)}$ .

**Special Case 1 (MC-I):** Suppose that the entries of  $\mathbf{c}_u^{(o)}$  take binary values  $\{\pm 1/\sqrt{N_f}\}$ , where the factor  $\sqrt{N_f}$  is used for normalization. In fact, such a choice of  $\mathbf{c}_u^{(o)}$  also guarantees the maximum coding gain. From (24), we deduce that entries of  $\epsilon_u$  are either  $\pm(s_u - s'_u)$ , or,  $\frac{\pm 1 \pm j}{\sqrt{2}}(s_u - s'_u)$ , both of which have the same magnitude. It then follows that  $\Theta_{\epsilon_u}^{(u,l)} = N_f (s_u - s'_u)^2 \mathbf{I}_{M_{u,l}+1}$ . According to Lemma 1, MC-UWB with  $\mathbf{c}_u^{(o)}$  having  $\{\pm 1/\sqrt{N_f}\}$  entries not only guarantees full diversity but also enjoys maximum coding gain.

**Special Case 2 (MC-II):** Consider here that the orthonormal codes are chosen as  $\mathbf{c}_u^{(o)} = \mathbf{e}_u/\sqrt{N_f}$ ,  $\forall u \in [0, N_f - 1]$ . Evidently, such a choice of  $\mathbf{c}_u^{(o)}$  does not satisfy condition (25). In fact, it can be shown that the resulting diversity order for user  $u$  now becomes

$$G_{d,cp}^{(mc2)}(u) = \begin{cases} \frac{1}{2} \sum_{l=1}^L \min\{1, M_{u,l} + 1\} = L/2, & \text{if } u = 0, \text{ or, } u = \frac{N_f}{2}, \\ \frac{1}{2} \sum_{l=1}^L \min\{\mathcal{D}_{u,l}, M_{u,l} + 1\} \in [L/2, L], & \text{otherwise.} \end{cases} \quad (26)$$

As with Walsh-Hadamard DS codes, the diversity order in this MC-II case becomes user (or, code) dependent, and full diversity can not be guaranteed, since  $G_{d,cp}^{(mc2)}(u) \leq G_{d,max}$ . We summarize these results in the following proposition.

**Proposition 2:** In a UWB system with parameters  $N_f$ ,  $T_f$ , and  $T_p$ , and  $L$ -finger RAKE with delays  $\{\tau(l)\}_{l=1}^L$  spaced at least  $2T_p$  apart, the achievable diversity order depends on the spreading code, when IBI is removed with CP. Specifically,

- 1) DS-UWB generally does not guarantee  $G_{d,max}$ ; e.g., with Walsh-Hadamard codes,  $G_{d,cp}^{(ds)}(u) \leq G_{d,max}$  as in (22) is user/code dependent.
- 2) ASC-UWB using  $\mathbf{G}_{sc}$  with carriers as in (2) achieves maximum diversity order  $G_{d,cp}^{(sc)} = G_{d,max}$ .
- 3) C-UWB guarantees  $G_{d,max}$ , if and only if (25) is satisfied.
- 4) In MC-UWB, if (25) is satisfied and  $|[c_u^{(o)}]_n + j[c_u^{(o)}]_{N_f-n}|$  stays invariant  $\forall n$ , then MC-UWB achieves both the maximum diversity order  $G_{d,max}$ , and the maximum coding gain  $G_{c,max}$ .

To corroborate these results, let us first recall that the diversity gain relies on the number of non-zero entries of  $\mathbf{F}_{N_f} \mathbf{c}_u$ . Since  $\mathbf{F}_{N_f} \mathbf{c}_u$  is nothing but the frequency response of the spreading codes, it is not surprising that MC-I codes guarantee  $G_{d,max}$ , while MC-II codes do not. Indeed, under MC-I, each user utilizes all carriers; where under MC-II, each user actually utilizes a single carrier. But interestingly, with carriers as in (2), SC-UWB enables  $G_{d,max}$  even with a single carrier, thanks to its multi-band signaling characteristic, and the critical  $0.5/N_f$  shift in its digital frequencies  $\{f_u\}_{u=0}^{N_u-1}$ . Insofar as coding gains,  $G_{c,max}$  can be achieved if and only if entries of  $\mathbf{F}_{N_f} \mathbf{c}_u$  share the same magnitude.

In a nutshell, for a given spreading gain  $N_f$ , single-user performance heavily depends on the UWB spreading code selection. Existing DS codes do not guarantee  $G_{d,max}$  when CP guards are employed. Even with ZP guards, the error performance with DS codes is suboptimum as  $G_{c,max}$  is not guaranteed. On the other hand, our novel SC/MC codes enable maximum diversity order, with ZP or CP guards. In particular, MC-UWB can also achieve (approach)  $G_{c,max}$  with CP (ZP) guards.

Next, we will investigate usage of our MC codes in a multi-access setup. Relying on low-complexity single-user RAKE re-

ception, we will show how MC-UWB affects MUI mitigation.

## V. MULTI-USER INTERFERENCE MITIGATION

In multi-access scenarios, employment of multiuser detection (MUD) approaches (e.g., such as ML ones) generally require knowledge of all users' channels and spreading codes, which is often unrealistic. Moreover, the computational complexity may be prohibitive for the stringent size and power limitations of UWB radios. Relying on simple receiver processing with RAKE reception, we will focus on *single-user matched filter* (MF)-RAKE detection using maximum ratio combining (MRC).

Collecting outputs of the RAKE correlators,  $L$  per frame, the I/O relationship is given by [c.f. (14) and (15)]

$$\begin{aligned} \mathbf{y} &= \sqrt{\frac{\mathcal{E}_\mu}{N_f}} \mathbf{H}_\mu \nu_\mu + \sum_{u \neq \mu} \sqrt{\frac{\mathcal{E}_u}{N_f}} \mathbf{H}_u \nu_u + \eta \\ &= \sqrt{\frac{\mathcal{E}_\mu}{N_f}} \mathbf{H}_\mu \mathbf{c}_\mu s_\mu + \sum_{u \neq \mu} \sqrt{\frac{\mathcal{E}_u}{N_f}} \mathbf{H}_u \mathbf{c}_u s_u + \eta, \end{aligned} \quad (27)$$

where  $\mathbf{y} = \mathbf{y}_{zp}$  and  $\mathbf{H}_u = \tilde{\mathbf{H}}_u$  with ZP, and  $\mathbf{y} = \mathbf{y}_{cp}$  and  $\mathbf{H}_u = \tilde{\mathbf{H}}_u$  with CP. With combining weights  $\beta_\mu$ , the decision statistic for detecting the symbol  $s_\mu$  is  $z_\mu := \beta_\mu^T \mathbf{y}$ .

Corresponding to MRC, MF combining weights for RAKE reception are given by  $\beta_\mu^{mf} := \sqrt{1/N_f} \mathbf{H}_\mu \mathbf{c}_\mu$ . Merging the desired and interfering user terms, the decision statistic after MF combining in the absence of noise becomes

$$\begin{aligned} (\beta_\mu^{mf})^T \mathbf{y} &= \frac{\sqrt{\mathcal{E}_\mu}}{N_f} \sum_{u=0}^{N_u-1} \mathbf{c}_\mu^T \mathbf{H}_\mu^T \mathbf{H}_u \mathbf{c}_u s_u \\ &= \frac{\sqrt{\mathcal{E}_\mu}}{N_f} \sum_{u=0}^{N_u-1} \sum_{l=1}^L \mathbf{c}_\mu^T \mathbf{H}_{\mu,l}^T \mathbf{H}_{u,l} \mathbf{c}_u s_u. \end{aligned} \quad (28)$$

In general, MF-RAKE does not guarantee MUI elimination. But if CP is coupled with MC spreading codes, it becomes possible to mitigate MUI even with low complexity MF-RAKE. In fact, we will see that special choices of  $\{\mathbf{c}_u^{(o)}\}_{u=0}^{N_f-1}$  can suppress MUI significantly, while maintaining the capability of simultaneously accommodating  $N_u = N_f$  active users.

To confirm this, we prove in Appendix IV that when  $\mathbf{c}_u^{(o)} = \mathbf{e}_u, \forall u \in [0, N_f - 1]$ , the decision statistic in (28) boils down to

$$(\beta_\mu^{mf})^T \mathbf{y} = \begin{cases} \sqrt{\mathcal{E}_\mu} \sum_{l=1}^L [\mathbf{d}_{\mu,\mu,l}]_\mu s_\mu, & \mu = 0, \text{ or, } \mu = N_f/2, \\ \sqrt{\mathcal{E}_\mu} \sum_{l=1}^L \left[ \begin{array}{l} \mathcal{R}([\mathbf{d}_{\mu,\mu,l}]_\mu) s_\mu + \\ \mathcal{I}([\mathbf{d}_{\mu,N_f-\mu,l}]_\mu) s_{N_f-\mu} \end{array} \right], & \text{otherwise,} \end{cases} \quad (29)$$

where  $\mathbf{d}_{\mu,u,l}$  consists of the element-by-element product of vectors  $\sqrt{N_f} \mathbf{F}_{0:M_{\mu,l}}^* \boldsymbol{\alpha}_{\mu,l}$  and  $\sqrt{N_f} \mathbf{F}_{0:M_{u,l}} \boldsymbol{\alpha}_{u,l}$ .

Surprisingly, (29) implies that even with simple MF-RAKE, the number of interfering users is reduced to at most one, as

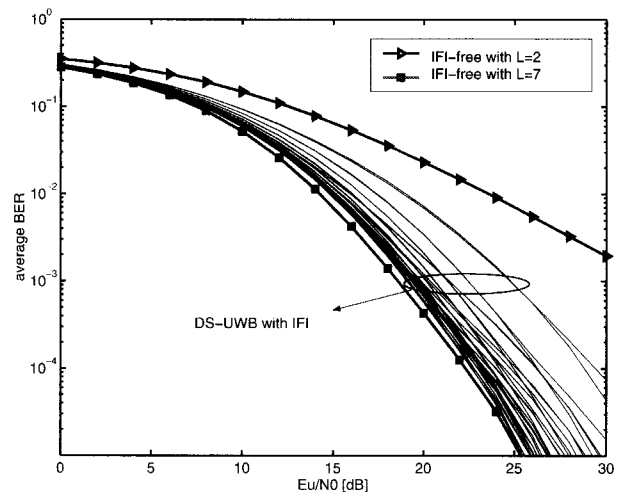


Fig. 3. Code-dependent DS-UWB performance with ZP guards and IFI; average BER corresponding to 32 individual codes is shown;  $\tau_u(L_u) = 90$  ns,  $T_f = 24$  ns,  $L = 2$  with IFI,  $M_{u,1} = 3$ , and  $M_{u,2} = 2$ .

opposed to  $N_f - 1$ . As a result, with low-cost UWB receivers equipped with MF-RAKE, our MC-UWB can accommodate  $(N_f/2 + 1)$  users while still achieving *single-user* performance; whereas with DS-UWB, single-user performance can be achieved only when 1 user is active. In typical UWB systems with large  $N_f$ , this translates to a significant user capacity increase by  $N_f/2$ .

Reducing the number of interfering users also reduces considerably the complexity of ML detection, and renders it feasible for UWB applications. Notice that this selection corresponds to our MC-II codes in Section IV, where we assign to each user a single real digital carrier. As mentioned before, full diversity is not guaranteed in this case. With each user employing more than one digital carriers, the diversity order can be increased at the price of reduced user capacity, or, increased MUD complexity. But certainly distinct from narrowband OFDMA that has diversity order 1, even with a single carrier (from the set of digital carriers in (6)), the minimum achievable diversity order is already  $L/2$ , as shown in (26).

**Remark:** We have derived a MF-RAKE model for digital receiver processing of UWB transmissions. Recall that in the development of our digital model, we did not impose any constraints on the number, or the placement of RAKE fingers. MF weights were developed also in [15], [11], by oversampling the received waveform. We have shown here that frame-rate RAKE reception can be implemented with analog waveforms, without oversampling. Specifically, the decision statistic  $z_\mu$  can be generated by correlating  $r(t)$  with the template  $\bar{p}_{\mu,n}(t)$  and sampling its output once per frame. The template is given by  $\bar{p}_{\mu,n}(t) = \sum_{l=1}^L [\beta_\mu]_{nL+l-1} p(t - \tau(l))$  during the  $n$ th frame, where  $n \in [0, N_1 - 1]$  with ZP, and  $n \in [M_1, N_1 - 1]$  with CP.

## VI. SIMULATIONS

In this section, we present simulations and comparisons to test our spreading codes, and validate our performance analysis in both single-user and multi-user scenarios. We select  $p(t)$



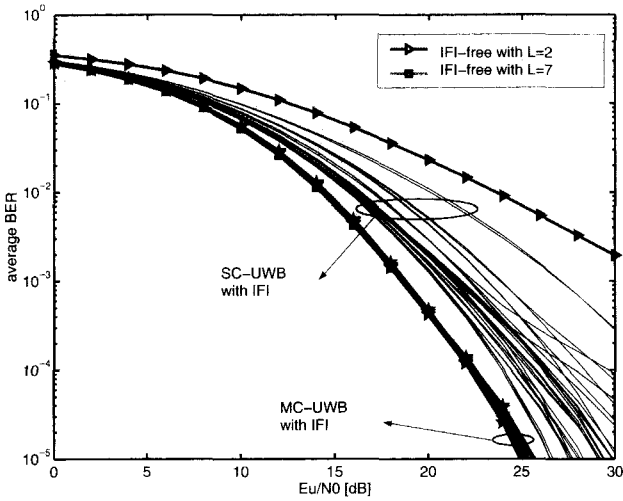


Fig. 4. Code-dependent SC-UWB performance with ZP guards and IFI; average BER corresponding to 32 individual codes (digital carriers) is shown;  $\tau_u(L_u) = 90$  ns,  $T_f = 24$  ns,  $L = 2$  with IFI,  $M_{u,1} = 3$ , and  $M_{u,2} = 2$ .

as the 2nd derivative of the Gaussian function with unit energy, and  $T_p \approx 1.0$  ns. Each symbol contains  $N_f = 32$  frames, each with  $T_f = 24$  ns. The random channels are generated according to [16], with parameters  $(1/\Lambda, 1/\lambda, \Gamma, \gamma) = (2, 0.5, 30, 5)$  ns. The resulting maximum delay spread of the multipath channel is 90 ns. The RAKE receiver uses  $L = 2$  fingers per frame, selected randomly but kept fixed for all testing scenarios. Consequently, we have  $M_{\mu,1} = 3$ , and  $M_{\mu,2} = 2$ , where  $\mu$  is the index of the desired user. Accounting for the ZP or CP guard of length  $M_1 = 3$ , the transmission rate is about 1.2Mbps for binary PAM.

According to Lemma 1, the maximum achievable diversity order is  $G_{d,max} = \frac{1}{2} \sum_{l=1}^L (M_{\mu,l} + 1) = 7/2$ , which is the same as that of a system with  $L = 7$  fingers but free from IFI. In the presence of IFI, DS-, and SC-UWB may result in diversity order as low as 1, which coincides with that of a system with  $L = 2$  fingers in the absence of IFI. Therefore, BER curves corresponding to these two IFI-free systems are also plotted as benchmarks. According to Corollary 1, these benchmark curves exhibit both  $G_{d,max}$  and  $G_{c,max}$ .

ML detection is applied to decode individual users with both ZP and CP guards. Average BER vs.  $\mathcal{E}_u/N_0$  with ZP is shown in Figs. 3 and 4, for DS, SC, and MC codes. Walsh-Hadamard codes are used for DS-UWB spreading and also for the  $c_u^{(\circ)}$  part of our MC-UWB codes, unless otherwise specified. Although all spreading codes can enable  $G_{d,max} = 7/2$ , the BER curves corresponding to all 32 MC spreading codes are almost identical to this  $L = 7$  benchmark performance (see Fig. 4); whereas those of the other two are distributed over a rather wide range (see Figs. 3 and 4). The performance difference between them comes from the discrepancy in their corresponding coding gains. Although the coding gain corresponding to MC-UWB is not maximum, it comes very close to  $G_{c,max}$ .

With CP, the average BER is shown in Figs. 5–7, for DS-, SC-, and MC-UWB (the special case of MC-II codes is also plotted). We observe that MC-UWB with  $L = 2$  RAKE fingers

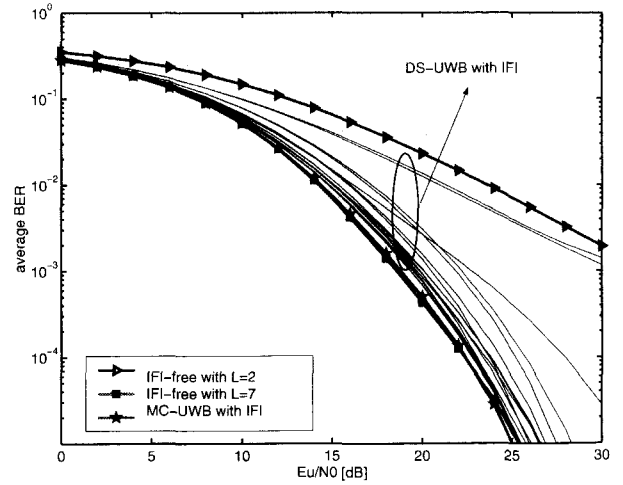


Fig. 5. Code-dependent DS-UWB performance with CP guards and IFI; average BER corresponding to 32 individual codes is shown;  $\tau_u(L_u) = 90$  ns,  $T_f = 24$  ns,  $L = 2$  with IFI,  $M_{u,1} = 3$ , and  $M_{u,2} = 2$ .

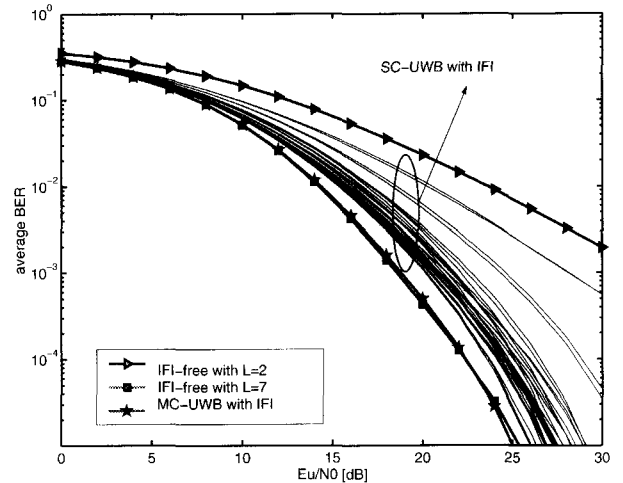


Fig. 6. Code-dependent SC-UWB performance with CP guards and IFI; average BER corresponding to 32 individual codes (digital carriers) is shown.  $\tau_u(L_u) = 90$  ns,  $T_f = 24$  ns,  $L = 2$  with IFI,  $M_{u,1} = 3$ , and  $M_{u,2} = 2$ .

in the presence of IFI yields BER curves identical to the  $L = 7$  benchmark without IFI; SC-UWB guarantees full diversity, but not maximum coding gain; DS-UWB enjoys full diversity for most users, but for some users it exhibits diversity order of only 1, as we predicted in (22); and MC-II exhibits diversity orders ranging from 1 to 2, as we predicted in (26). In Fig. 8, the BER averaged over all codes is also plotted, where MC-UWB is confirmed to outperform all other spreading codes.

With IFI being removed by CP guards, Fig. 9 depicts BER of MF-RAKE detectors, in multi-access UWB operation under variable user loads: fully loaded with  $N_u = 32$  users (dashed curves), medium loaded with  $N_u = 17$  users (solid curves), and lightly loaded with  $N_u = 1$  (dotted curves). Under light user loads MC-UWB outperforms all others. In the medium loaded system, the performance of MC-II codes is identical to the single-user case, as expected. In the fully loaded case, all of them exhibit error floor. Among all spreading codes, MC-UWB

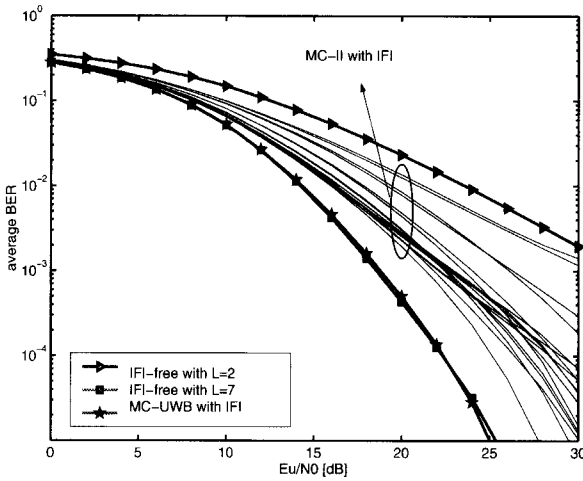


Fig. 7. Code-dependent MC-II performance with CP guards and IFI; average BER corresponding to 32 individual codes is shown;  $\tau_u(L_u) = 90$  ns,  $T_f = 24$  ns,  $L = 2$  with IFI,  $M_{u,1} = 3$ , and  $M_{u,2} = 2$ .

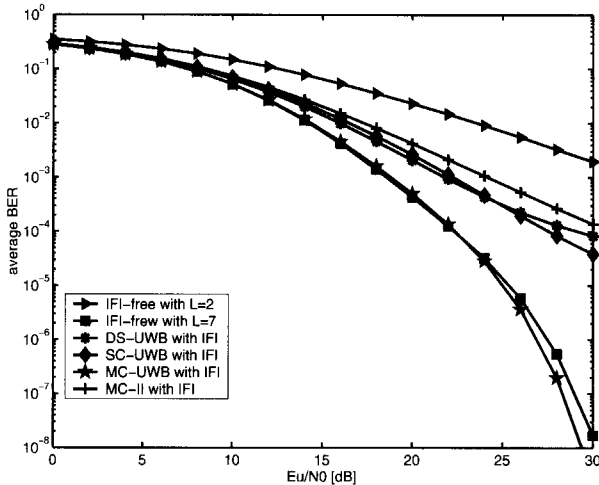


Fig. 8. CP for IFI removal;  $\tau_u(L_u) = 90$  ns,  $T_f = 24$  ns,  $L = 2$ ,  $M_{u,1} = 3$ , and  $M_{u,2} = 2$ .

exhibits highest sensitivity to MUI, possibly because all users have identically flat transmit spectra. For these (even close to) fully loaded systems, the single user RAKE receivers motivated here by complexity considerations are not sufficient to cope with the near-far effects that cause the error floors in Fig. 9. For these fully loaded cases, our spreading codes in [6] are well motivated because they are capable of eliminating MUI by design, while being able to afford single-user complexity.

## VII. CONCLUSIONS

In this paper, we introduced two real-valued spreading codes (SC and MC), for baseband UWB multiple access. Constructed using discrete cos/sin functions, our SC/MC codes can be implemented with low-complexity DCT circuits. Relative to DS-UWB, SC-UWB and MC-UWB offer flexibility in handling NBI, simply by avoiding the corresponding digital carriers. Moreover, utilizing single or multiple digital carriers, these codes have multi-band UWB spectra. Consequently, different

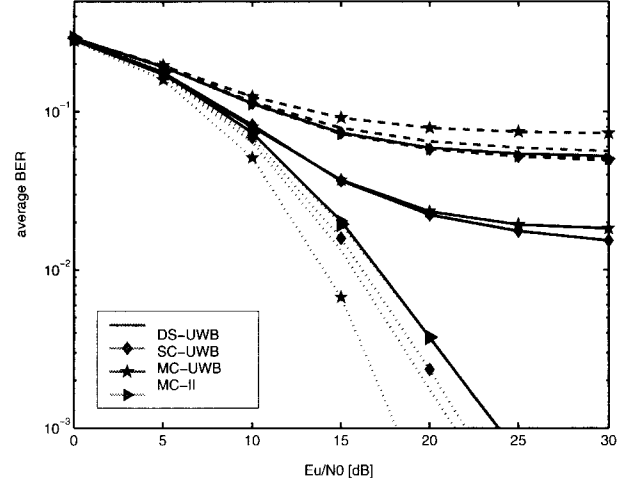


Fig. 9. BER performance of MUD with MF, and CP used for IFI removal. Dashed, solid, and dotted curves correspond to cases with  $N_u = 32$ ,  $N_u = 17$ , and  $N_u = 1$ , respectively;  $\tau_u(L_u) = 90$  ns,  $T_f = 24$  ns,  $L = 2$  with IFI.

from narrowband OFDMA systems, each SC-UWB user occupies multiple frequency bands, and enjoys full multipath diversity, even with a single digital carrier. In addition, MC-UWB achieves maximum coding gain. Finally, even with frame-rate samples and simple matched filtering operations, SC- and MC-UWB are capable of reducing multi-user interference, which in turn reduces receiver complexity.

## APPENDICES

### I. Proof of (18)

Let us first consider the ZP option. Recalling the block structure of  $\tilde{\mathbf{H}}_u$  with ZP and  $\tilde{\mathbf{H}}_u$  with CP, we deduce that  $d^2(\tilde{\mathbf{y}}, \tilde{\mathbf{y}}') = \frac{\mathcal{E}_u}{N_f} \epsilon^2 \sum_{l=1}^L \epsilon_u^T \tilde{\mathbf{H}}_{u,l}^T \tilde{\mathbf{H}}_{u,l} \epsilon_u$ . Since the product of a Toeplitz matrix with a vector represents a convolution between two vectors, and convolution is commutative, it follows that  $\tilde{\mathbf{H}}_{u,l} \epsilon_u = \mathbf{E}_{u,l} \alpha_{u,l}$ , where  $\mathbf{E}_{u,l}$  is a  $N_f \times (M_{u,l} + 1)$  Toeplitz matrix with first column  $[\epsilon_u(0), \dots, \epsilon_u(N_f - 1), 0, \dots, 0]^T$ . As a result,

$$d^2(\tilde{\mathbf{y}}, \tilde{\mathbf{y}}') = \frac{\mathcal{E}_u}{N_f} \sum_{l=1}^L \alpha_{u,l}^T \mathbf{E}_{u,l}^T \mathbf{E}_{u,l} \alpha_{u,l}. \quad (30)$$

Likewise with CP, we have  $d^2(\tilde{\mathbf{y}}, \tilde{\mathbf{y}}') = \frac{\mathcal{E}_u}{N_f} \sum_{l=1}^L \epsilon_u^T \tilde{\mathbf{H}}_{u,l}^T \tilde{\mathbf{H}}_{u,l} \epsilon_u$ . Being circulant,  $\tilde{\mathbf{H}}_{u,l}$  can be diagonalized by FFT matrices as  $\mathbf{D}_{H_{u,l}} := \mathbf{F}_{N_f} \tilde{\mathbf{H}}_{u,l} \mathbf{F}_{N_f}^H$ . It can be verified that  $\mathbf{D}_{H_{u,l}} = \text{diag}\{\sqrt{N_f} \mathbf{F}_{0:M_{u,l}} \alpha_{u,l}\}$ , where  $\mathbf{F}_{0:m}$  denotes the matrix formed by the first  $(m + 1)$  columns of  $\mathbf{F}_{N_f}$ . Defining  $\epsilon_u := \mathbf{F}_{N_f} \epsilon_u$ , and letting  $\mathbf{D}_{\epsilon_u} := \text{diag}\{\epsilon_u\}$ , we have  $\forall l \in [1, L]$

$$\begin{aligned} \epsilon_u^T \tilde{\mathbf{H}}_{u,l}^T \tilde{\mathbf{H}}_{u,l} \epsilon_u &= \epsilon_u^T \mathbf{F}_{N_f}^H \mathbf{D}_{H_{u,l}} \mathbf{D}_{H_{u,l}} \mathbf{F}_{N_f} \epsilon_u \\ &= N_f \alpha_{u,l}^T \mathbf{F}_{0:M_{u,l}}^H \mathbf{D}_{\epsilon_u} \mathbf{D}_{\epsilon_u} \mathbf{F}_{0:M_{u,l}} \alpha_{u,l}. \end{aligned} \quad (31)$$

Summarizing (30) and (31), the Euclidean distance between  $\tilde{\mathbf{y}}$  and  $\tilde{\mathbf{y}}'$  is given by:  $d^2(\tilde{\mathbf{y}}, \tilde{\mathbf{y}}') = \frac{\mathcal{E}_u}{N_f} \sum_{l=1}^L \alpha_{u,l}^T \Theta_{\epsilon_u}^{(u,l)} \alpha_{u,l}$ ,

where  $\Theta_{\varepsilon_u}^{(u,l)} = \mathbf{E}_{u,l}^T \mathbf{E}_{u,l}$  in the ZP case, and  $\Theta_{\varepsilon_u}^{(u,l)} = N_f \mathbf{F}_{0:M_{u,l}}^H \mathbf{D}_{\varepsilon_u}^H \mathbf{D}_{\varepsilon_u} \mathbf{F}_{0:M_{u,l}}$  in the CP case. Substituting into (16), we obtain (18).

## II. Proof of (19)

Since UWB systems employ real signals, we are only interested in the real part of each path gain, which we model as zero-mean Gaussian distributed. As combinations of Gaussian random variables,  $\alpha_{u,l}(n)$ 's are also zero-mean Gaussian. Moreover, if the finger delays are chosen such that  $\tau(l) - \tau(l-1) \geq 2T_p, \forall l \in [2, L]$ , the resultant  $\alpha_{u,l}(n)$ 's are uncorrelated.

With  $\alpha_{u,l}(n)$  being zero-mean, uncorrelated Gaussian, with variance  $\mathcal{A}_{u,l}(n) = \mathbb{E}\{\alpha_{u,l}^2(n)\}$ , the average PEP can be upper bounded by [c.f. (18)]

$$P(\nu_u \rightarrow \nu'_u) \leq \prod_{l=1}^L \prod_{m=0}^{M_{u,l}} \left[ 1 + \frac{\mathcal{E}_u}{N_f} \frac{\mathcal{A}_{u,l}(m) \lambda_{\varepsilon_u}^{(u,l)}(m)}{2N_0} \right]^{-1/2}, \quad (32)$$

where  $\{\lambda_{\varepsilon_u}^{(u,l)}(m)\}_{m=0}^{M_{u,l}}$  are the nonincreasing eigenvalues of the matrix  $\Theta_{\varepsilon_u}^{(u,l)} := \mathbf{E}_{u,l}^T \mathbf{E}_{u,l}$ . Letting  $r_{\varepsilon_u}^{(u,l)}$  denote the rank of  $\Theta_{\varepsilon_u}^{(u,l)}$ , it follows that  $\lambda_{\varepsilon_u}^{(u,l)}(m) \neq 0$  if and only if  $m \in [0, r_{\varepsilon_u}^{(u,l)} - 1]$ . At high SNR ( $\mathcal{E}_u/N_0 \gg 1$ ), (32) becomes

$$P(\nu_u \rightarrow \nu'_u) \leq \left( \frac{\mathcal{E}_u}{2N_0} \right)^{-\frac{1}{2} \sum_{l=1}^L r_{\varepsilon_u}^{(u,l)}} \times \left[ \prod_{l=1}^L \prod_{m=0}^{r_{\varepsilon_u}^{(u,l)}-1} \frac{\mathcal{A}_{u,l}(m) \lambda_{\varepsilon_u}^{(u,l)}(m)}{N_f} \right]^{-1/2}.$$

## III. Proof of Lemma 1

By checking the dimensionality of  $\{\Theta_{\varepsilon_u}^{(u,l)}\}_{l=1}^L$ , it is clear that the maximum diversity order is  $G_{d,max} = \frac{1}{2} \sum_{l=1}^L (M_{u,l} + 1)$ , which is achieved when  $\Theta_{\varepsilon_u}^{(u,l)}$  is full rank,  $\forall l \in [1, L]$ , and  $\forall \varepsilon_u \neq \mathbf{0}$ .

In this case, the coding gain corresponding to  $\varepsilon_u$  turns out to be

$$G_{c,\varepsilon} := \left[ \prod_{l=1}^L \det \left\{ \Theta_{\varepsilon_u}^{(u,l)} \right\} \prod_{m=0}^{M_{u,l}} \frac{\mathcal{A}_{u,l}(m)}{N_f} \right]^{1/(2G_{d,max})}. \quad (33)$$

To find the maximum determinant of  $\Theta_{\varepsilon_u}^{(u,l)}$ , let us first look at its trace.

In the ZP case,  $\Theta_{\varepsilon_u}^{(u,l)} = \mathbf{E}_{u,l}^T \mathbf{E}_{u,l}$ . Recalling that  $\nu_u = s_u \mathbf{c}_u$ , we have  $\varepsilon_u = (s_u - s'_u) \mathbf{c}_u$ . With  $\mathbf{E}_{u,l}^T$  being Toeplitz matrices and  $\mathbf{c}_u^T \mathbf{c}_u = N_f$ , it can be easily verified that the  $(M_{u,l} + 1)$  diagonal entries of  $\Theta_{\varepsilon_u}^{(u,l)}$  are all given by  $N_f (s_u - s'_u)^2$ .

In the CP case,  $\Theta_{\varepsilon_u}^{(u,l)} = N_f \mathbf{F}_{0:M_{u,l}}^H \mathbf{D}_{\varepsilon_u}^H \mathbf{D}_{\varepsilon_u} \mathbf{F}_{0:M_{u,l}}$ . Since  $\varepsilon_u = \mathbf{F}_{N_f} \varepsilon_u = (s_u - s'_u) \mathbf{F}_{N_f} \mathbf{c}_u$ , the  $(n+1)$ st diagonal entry of  $\mathbf{D}_{\varepsilon_u}^H \mathbf{D}_{\varepsilon_u}$  is nothing but  $(s_u - s'_u)^2 |\mathbf{f}_n^T \mathbf{c}_u|^2$ . Consequently, the diagonal entries of  $\Theta_{\varepsilon_u}^{(u,l)}$  are given by:  $N_f (s_u - s'_u)^2 \frac{1}{N_f} \sum_{n=0}^{N_f-1} |\mathbf{f}_n^T \mathbf{c}_u|^2 = (s_u - s'_u)^2 \mathbf{c}_u^T \mathbf{F}_{N_f} \mathbf{F}_{N_f}^H \mathbf{c}_u =$

$N_f (s_u - s'_u)^2$ , which coincide with these of the ZP case. This is not surprising, because both cases are subject to the same energy constraint.

The trace of  $\Theta_{\varepsilon_u}^{(u,l)}$  is  $\text{tr}\{\Theta_{\varepsilon_u}^{(u,l)}\} = (M_{u,l} + 1)N_f (s_u - s'_u)^2$ , in both ZP and CP cases. Because  $\Theta_{\varepsilon_u}^{(u,l)}$  is positive definite, we have  $\det\{\Theta_{\varepsilon_u}^{(u,l)}\} \leq [N_f (s_u - s'_u)^2]^{M_{u,l}+1}$ , where equality is achieved if and only if  $\lambda_{\varepsilon_u}^{(u,l)}(m) = N_f (s_u - s'_u)^2, \forall m \in [0, M_{u,l}]$ . It then follows that  $\min_{\varepsilon \neq \mathbf{0}} \left\{ \det\{\Theta_{\varepsilon_u}^{(u,l)}\} \right\} \leq (N_f d_{min}^2)^{M_{u,l}+1}$ , where  $d_{min}$  denotes the minimum Euclidean distance among all possible values of  $s_u$ . The resulting maximum coding gain is  $G_{c,max} := d_{min}^2 \left[ \prod_{l=1}^L \prod_{m=0}^{M_{u,l}} \mathcal{A}_{u,l}(m) \right]^{1/(2G_{d,max})}$ .

## IV. Proof of (29)

If MC spreading codes are employed, and CP is used to remove IBI, then we have

$$\begin{aligned} & \mathbf{c}_\mu^T \tilde{\mathbf{H}}_{\mu,l}^T \tilde{\mathbf{H}}_{u,l} \mathbf{c}_u \\ &= \mathbf{c}_\mu^{(o)T} \mathbf{G}_{\mu,l}^T \tilde{\mathbf{H}}_{\mu,l}^T \tilde{\mathbf{H}}_{u,l} \mathbf{G}_{u,l} \mathbf{c}_u^{(o)} \\ &= \mathbf{c}_\mu^{(o)T} \mathbf{G}_{\mu,l}^T \mathbf{F}_{N_f}^H \mathbf{D}_{H_{\mu,l}}^H \mathbf{D}_{H_{u,l}} \mathbf{F}_{N_f} \mathbf{G}_{u,l} \mathbf{c}_u^{(o)}. \end{aligned} \quad (34)$$

Let the  $N_f \times 1$  vector  $\mathbf{d}_{\mu,u,l}$  denote the diagonal entries of the product  $\mathbf{D}_{H_{\mu,l}}^H \mathbf{D}_{H_{u,l}}$ . It can be shown that the  $(m+1, n+1)$ st entry of the product  $\Psi_{\mu,u,l} := \mathbf{G}_{\mu,l}^T \mathbf{F}_{N_f}^H \mathbf{D}_{H_{\mu,l}}^H \mathbf{D}_{H_{u,l}} \mathbf{F}_{N_f} \mathbf{G}_{u,l}$  is given  $\forall m, n \in [0, N_f - 1]$  by [c.f. (24)]

$$[\Psi_{\mu,u,l}]_{m,n} = \begin{cases} N_f [\mathbf{d}_{\mu,u,l}]_n \delta(m-n), & n=0, \text{ or } n = \frac{N_f}{2}, \\ N_f \left[ \mathcal{R}([\mathbf{d}_{\mu,u,l}]_n) \delta(m-n) + \mathcal{I}([\mathbf{d}_{\mu,u,l}]_n) \delta(m+n-N_f) \right], & \text{otherwise.} \end{cases}$$

It is clear that pre- and post-multiplication with generic orthonormal sequences  $\mathbf{c}_\mu^{(o)}$  and  $\mathbf{c}_u^{(o)}$  does not eliminate cross-user ( $\mu \neq u$ ) terms.

But with  $\mathbf{c}_u^{(o)} = \mathbf{e}_u, \forall u$ , (34) becomes

$$\begin{aligned} & \mathbf{c}_\mu^T \tilde{\mathbf{H}}_{\mu,l}^T \tilde{\mathbf{H}}_{u,l} \mathbf{c}_u \\ &= \begin{cases} N_f [d_{\mu,u,l}]_n \delta(u-\mu), & \mu=0, \text{ or } \mu = \frac{N_f}{2}, \\ N_f \left[ \mathcal{R}([\mathbf{d}_{\mu,u,l}]_n) \delta(u-\mu) + \mathcal{I}([\mathbf{d}_{\mu,u,l}]_n) \delta(u+\mu-N_f) \right], & \text{otherwise.} \end{cases} \end{aligned}$$

The decision statistic after MF combining in the absence of noise now translates to (29).

## REFERENCES

- [1] M. Z. Win and R. A. Scholtz, "Ultra wide bandwidth time-hopping spread-spectrum impulse radio for wireless multiple access communications," *IEEE Trans. Commun.*, vol. 48, no. 4, pp. 679–691, Apr. 2000.
- [2] J. R. Foerster, "The performance of a direct-sequence spread ultra wide-band system in the presence of multipath, narrowband interference, and multiuser interference," in *Proc. IEEE Conf. Ultra Wideband Systems and Technologies*, Baltimore, MD, USA, May 20–23, 2002, pp. 87–92.

- [3] B. M. Sadler and A. Swami, "On the performance of UWB and DS-spread spectrum communication systems," in *Proc. IEEE Conf. on Ultra Wideband Systems and Technologies*, Baltimore, MD, May 20–23, 2002, pp. 289–292.
- [4] R. A. Scholtz, "Multiple access with time-hopping impulse modulation," in *Proc. MILCOM Conf.*, Boston, MA, USA, Oct. 11–14, 1993, pp. 447–450.
- [5] H. Sari and G. Karam, "Orthogonal frequency-division multiple access and its application to catv network," *ETT*, vol. 9, pp. 507–516, Nov./Dec. 1998.
- [6] L. Yang and G. B. Giannakis, "Multi-stage block-spreading for impulse radio multiple access through ISI channels," *IEEE J. Select. Areas Commun.*, vol. 20, no. 9, pp. 1767–1777, Dec. 2002.
- [7] J. Proakis, *Digital Communications*, McGraw-Hill, New York, 4th ed., Feb. 2001.
- [8] Z. Wang, "Multi-carrier ultra-wideband multiple-access with good resilience against multiuser interference," in *Proc. Conf. Info. Sciences & Systems*, Baltimore, MD, Mar. 12–14, 2003.
- [9] M. Z. Win and R. A. Scholtz, "On the energy capture of ultrawide bandwidth signals in dense multipath environments," *IEEE Commun. Lett.*, vol. 2, no. 9, pp. 245–247, Sept. 1998.
- [10] D. Cassioli *et al.*, "Performance of low-complexity rake reception in a realistic uwb channel," in *Proc. Int. Conf. Commun.*, New York, NY, USA, Apr. 28–May 2, 2002, pp. 763–767.
- [11] G. Durisi, J. Romme, and S. Benedetto, "Performance of TH and DS UWB multiaccess systems in presence of multipath channel and narrow-band interference," in *Proc. International Workshop on Ultra Wideband Systems*, Oulu, Finland, June 2–5, 2003.
- [12] Z. Wang and G. B. Giannakis, "Complex-field coding for OFDM over fading wireless channels," *IEEE Trans. Inform. Theory*, vol. 49, no. 3, pp. 707–720, Mar. 2003.
- [13] Z. Wang and G. B. Giannakis, "A simple and general parameterization quantifying performance in fading channels," *IEEE Trans. Commun.*, vol. 51, no. 8, pp. 1389–1398, Aug. 2003.
- [14] L. Yang and G. B. Giannakis, "Analog space-time coding for multi-antenna ultra-wideband transmissions," *IEEE Trans. Commun.*, 2004 (to appear).
- [15] C. J. Le Martret and G. B. Giannakis, "All-digital impulse radio for wireless cellular systems," *IEEE Trans. Commun.*, vol. 50, no. 9, pp. 1440–1450, Sept. 2002.
- [16] A. A. M. Saleh and R. A. Valenzuela, "A statistical model for indoor multipath propagation," *IEEE J. Select. Areas Commun.*, vol. 5, no. 2, pp. 128–137, Feb. 1987.



Liuqing Yang received her B.S. degree in Electrical Engineering from the Huazhong University of Science and Technology, Wuhan, China, in 1994, and M.Sc. degree in Electrical Engineering from the University of Minnesota, in 2002. She is currently a Ph.D. candidate in the Department of Electrical and Computer Engineering, at the University of Minnesota. Her research interests include communications, signal processing, and networking. Currently, she has a particular interest in Ultra Wideband (UWB) communications. Her research encompasses synchronization, channel estimation, equalization, multiple access, space-time coding, and multicarrier systems.



Georgios B. Giannakis received his Diploma in Electrical Engineering from the National Technical University of Athens, Greece, 1981. From September 1982 to July 1986 he was with the University of Southern California (USC), where he received his MSc. in Electrical Engineering, 1983, MSc. in Mathematics, 1986, and Ph.D. in Electrical Engineering, 1986. After lecturing for one year at USC, he joined the University of Virginia in 1987, where he became a professor of Electrical Engineering in 1997. Since 1999 he has been a professor with the Department of Electrical and Computer Engineering at the University of Minnesota, where he now holds an ADC Chair in Wireless Telecommunications.

His general interests span the areas of communications and signal processing, estimation and detection theory, time-series analysis, and system identification – subjects on which he has published more than 175 journal papers, 325 conference papers, and two edited books. Current research focuses on transmitter and receiver diversity techniques for single- and multi-user fading communication channels, complex-field and space-time coding, multicarrier, ultra-wide band wireless communication systems, cross-layer designs, and distributed sensor networks.

G. B. Giannakis is the (co-) recipient of four best paper awards from the IEEE Signal Processing (SP) Society (1992, 1998, 2000, 2001). He also received the Society's Technical Achievement Award in 2000. He served as Editor in Chief for the *IEEE SP Letters*, as Associate Editor for the *IEEE Trans. on Signal Processing* and the *IEEE SP Letters*, as secretary of the SP Conference Board, as member of the SP Publications Board, as member and vice-chair of the Statistical Signal and Array Processing Technical Committee, as chair of the SP for Communications Technical Committee, and as a member of the IEEE Fellows Election Committee. He is currently a member of the IEEE-SP Society's Board of Governors, the Editorial Board for the *Proceedings of the IEEE*, and chairs the steering committee of the *IEEE Trans. on Wireless Communications*.